31st Congress of the International Council of the Aeronautical Sciences

Belo Horizonte, Brazil; September 09-14, 2018

MODELLING OF MIXED MODE FATIGUE-INDUCED DELAMINATION IN COMPOSITES: A COMPARATIVE STUDY

Lucas A. de Oliveira*, Douglas S. Alves*, Maurício V. Donadon*
***Instituto Tecnológico de Aeronáutica, Brazil**

Keywords: *Fatigue, Delamination, Cohesive Models, Composite*

Abstract

Three numerical models for the prediction of high-cycle fatigue-driven delamination in carbon/epoxy composite laminates are compered through finite element analysis of a mixed-mode bending specimen. These models allows delamination modelling without knowing, a priori, the modes ratios. The models are implemented into ABAQUS/Explicit FE code within solid elements. The local part (at element level) of the algorithms are implemented in a user-defined material subroutine (VUMAT) and the non-local part (at structure level), in a VEXTERNALDB subroutine. The study found that the use of strain energy release rate based on Paris' law variation combined with cohesive zone model is a robust approach. The use of strength-based damage parameter to account for the fatigue damage reduces the numerical integration error associated with the cycle jump and the non-local crack tip tracking algorithm improves the accuracy.

1 Introduction

The transportation industry faces the challenge to provide products that combine high safety requirements, quality, comfort and good design with the low fuel burn consumption in order to reduce the operational cost of their customers. In this context, the aerospace industry is expanding the application of composite materials from simple fairings, wardrobes and radomes to primary structural components such as fuselage and wings structures.

Fatigue-induced delamination is one of the possible failure modes when using laminated composite materials. Therefore, applying composite materials in primary structural elements of aircraft requires the development of numerical methods to predict failure modes in operational scenarios.

Robinson et al. [1] proposed a strain-based high cycle fatigue induced delamination models using Peerling's law [2]. Robinson's model uses numerical fitting parameters, which is calibrated simulating a coupon repeatedly and comparing with experimental data.

Turon, Costa, Camanho and Dávila [3] proposed a model using a Paris' law variation. The Paris' law parameters are fitted from the experimental data instead of the model itself. Therefore, the proposed model is straightforward and easily implemented. Moreover, it avoids the structure dependence of the strain-based models. Nevertheless, the model shows to be very sensitive to the cohesive zone length estimated by the closed-form equation proposed by Rice [4].

Harper and Hallett [5] proposed a strength-based fatigue delamination model that reduces the error associated with the numerical integration of the damage rate. Additionally, the authors studied in detail the cohesive zone and identified two different regions, a static dominated zone and a fatigue dominated one. In this case, the model accounts for the unwanted damage that occurs in another area other than in the fatigue zone. The authors also proposed a more accurate estimation of the cohesive zone length.

Kawashita and Hallett [6] improved the

model of Harper and Hallett [5] adding a crack tip tracking algorithm. This algorithm allows the authors to degrade only the elements at the crack tip, not interfering with the other elements in the cohesive zone, and, consequently, overcoming the need to estimate its length. Additionally, the authors proposed a estimation of the element effective length improving the model accuracy for a crack front growing in two directions. This work is the first to address this issue, while the previous others only account for one-directional crack growing. This model was also tested in an open hole specimen by Nixon-Pearson, Hallett, Harper and Kawashita [7].

This present work evaluates the performance of the three last models [3,5,6], applying them to a finite element analysis of a mixed-mode bending (MMB) specimen. To observe the performance of the fatigue part of each model only, the same quasi-static model is used for all models. The quasi-static model used is similar to the one presented in Ref. [8].

2 Constitutive Law

In the interlaminar fracture analysis, the constitutive law defines the traction-separation relationship between two adjacent layers. This law is based on the Cohesive Zone Model (CZM), as give by Eq. (1).

$$\begin{aligned} \sigma_I &= K(1-D_K)\langle\delta_I\rangle - K\langle-\delta_I\rangle \\ \sigma_{II} &= K(1-D_K)\delta_{II} \\ \sigma_{III} &= K(1-D_K)\delta_{III} \end{aligned} \tag{1}$$

where $\langle\cdot\rangle$ is the Macaulay brackets. The Eq. (1) has a single damage variable D_K which describes the material loss of stiffness for the three fracture modes. D_K is defined by Eq. (2).

$$D_K \equiv \frac{K^d}{K} = 1 - \frac{\tilde{K}}{K} \tag{2}$$

The variable D_K is composed of two damage parameters simultaneously computed, namely quasi-static damage parameter D_K^s and fatigue damage parameter D_K^f, as given by Eq. (3).

$$D_K = D_K^s + D_K^f \tag{3}$$

Further details on the expression of both static and fatigue damage parameters are provided in Sections 3 and 4, respectively.

3 Quasi-Static Delamination Model

In this present work, the bi-linear traction–separation law (TSL) describes the quasi-static damage evolution. The bi-linear TSL combines two behaviours, as shown in Fig. 1 for a generic mode loading. Starting from zero displacement, the material presents a linear elastic response until the displacement δ reaches the strength value S at the damage onset displacement δ^0. After the damage onset point, the behaviour consists of a linear softening response, which is representative of an averaged damage. In this softening curve, the stress starts from the strength value at the damage onset point and decreases to zero at the fully damaged displacement δ^f. After reaching the fully damaged displacement, the material can no longer sustain any load, and the stress remains zero.

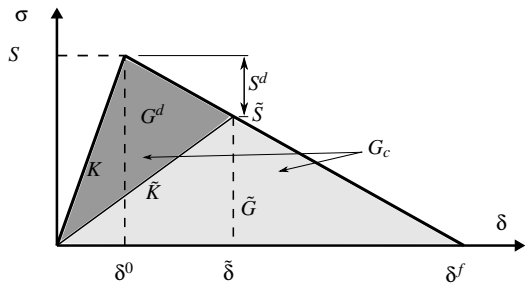

Fig. 1 Bi-linear traction–separation law for a generic mode loading

Based on this linear softening, the stiffness damage variable is defined as given by Eq. (4).

$$D_K = \frac{\delta^f}{\tilde{\delta}}\left(\frac{\tilde{\delta}-\delta^0}{\delta^f-\delta^0}\right) \tag{4}$$

Since the damage is irreversible, the damage variable D_K can not decrease. During unloading, D_k is not further increased and kept constant.

Furthermore, Eq. (4) is valid when the relative displacement is higher than the damage onset displacement and lower than the fully damaged displacement. Before the damage onset, the damage variable D_K value is zero and after the fully damaged displacement, is one.

In the CZM, The Strain Energy Release Rate (SERR), represented by G, is assumed being equal to the work w^s per unit of the Representative Volume Element (RVE) cross-sectional area. This specific work corresponds to the area below the curve in the traction-separation plot depicted in Fig. 2. Furthermore, the fully damaged displacement δ^f is chosen such that this RVE specific work is equal to the material fracture toughness G_c, as given by Eq. (5).

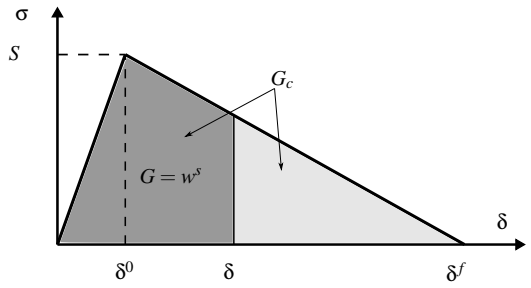

Fig. 2 Strain energy release rate

$$G_c = \frac{1}{2} S \delta^f \tag{5}$$

The SERR is obtained by integrating the traction-separation curve as follows.

$$G = w^s = \int_0^{\delta} \sigma \, d\delta = \frac{1}{2} S \left[\delta^f - \frac{\left(\delta^f - \delta\right)^2}{\delta^f - \delta^0} \right] \tag{6}$$

3.1 Mixed Mode Delamination

The model described above can be applied to mixed mode delamination using an equivalent traction-displacement curve as represented in Fig. 3. In this equivalent curve, the equivalent displacement δ_{eq} is obtained by Eq. (7). Furthermore, the damage onset displacement δ^0_{eq} is calculated using an interactive stress criterion and the fully damaged displacement δ^f_{eq} is calculated using an interactive energy criterion.

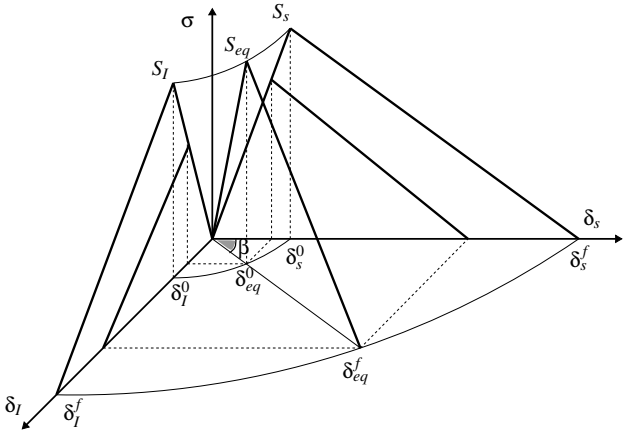

Fig. 3 Traction–separation for mixed mode delamination

$$\begin{aligned} \delta_{eq} &= \sqrt{\langle \delta_I \rangle^2 + {\delta_s}^2} \\ \delta_s &= \sqrt{{\delta_{II}}^2 + {\delta_{III}}^2} \end{aligned} \tag{7}$$

The equivalent damage onset displacement is calculated employing a quadratic stress-based criterion proposed by Ye [9].

$$\left(\frac{\langle \sigma_I \rangle}{S_I} \right)^2 + \left(\frac{\sigma_s}{S_s} \right)^2 = 1 \tag{8}$$

where S_I and S_s are the strengths associated with the pure mode I and shear mode delamination, respectively. Therefore, the equivalent damage onset displacement δ^0_{eq} is obtained by Eq. (9).

$$\begin{aligned} \delta^0_{eq} = \Bigg[&\left(\frac{\langle K_I \cos(\beta) \rangle}{S_I} \right)^2 \\ &+ \left(\frac{K_s \sin(\beta)}{S_s} \right)^2 \Bigg]^{-\frac{1}{2}} \end{aligned} \tag{9}$$

In a mixed mode loading, the equivalent fully damaged displacement δ^f_{eq} value is chosen in a way that the area below the equivalent traction-separation curve is equal to the equivalent critical $G_{eq,c}$. In order to determine this value, the Power-Law [10] SERR-based criterion is used.

$$\left(\frac{G_I}{G_{I,c}} \right)^{\lambda} + \left(\frac{G_s}{G_{s,c}} \right)^{\lambda} = 1 \tag{10}$$

where $G_s = G_{II} + G_{II}$ and $G_{s,c} = G_{II,c} = G_{III,c}$.

Therefore, the equivalent fully damaged displacement δ^f_{eq} is given by Eq. (11).

$$\delta^f_{eq} = \frac{2}{\delta^0_{eq}} \left[\left(\frac{K_I cos^2(\beta)}{G_{I,c}} \right)^{\lambda} + \left(\frac{K_s sin^2(\beta)}{G_{s,c}} \right)^{\lambda} \right]^{-\frac{1}{\lambda}} \tag{11}$$

4 Fatigue Models

The fatigue-driven delamination is commonly described in terms of an effective main crack growth rate $\frac{da}{dn}$, which is measured through extensive tests and expressed by a Paris' law variation written as a function of SERR variation ΔG for each mode ratio, as follows.

$$\frac{da}{dn} = C \left(\frac{\Delta G}{G_c} \right)^m \tag{12}$$

where the equation coefficients C and exponent m are experimentally determined parameters and ΔG is the SERR cyclic variation. This variation can be written in terms of maximum SERR G_{max} and load ratio R.

$$\Delta G = G_{max} \left(1 - R^2\right) \tag{13}$$

In a mixed mode fatigue-driven delamination, the Paris' law coefficient and exponent need to be interpolated from measured mode ratio. This is performed using the formulation proposed by Blanco, Gamstedt, Asp and Costa [11].

$$m = m_I + m_b \phi_s + (m_s - m_I - m_b) (\phi_s)^2 \tag{14}$$

$$\log(C) = \log(C_I) + \log(C_b)\phi_s + \log\left(\frac{C_s}{C_I C_b}\right) (\phi_s)^2 \tag{15}$$

where ϕ_s is the mode ratio.

$$\phi_s = \frac{G_{II} + G_{II}}{G_I + G_{II} + G_{III}} \tag{16}$$

This formulation presents one fitting parameter for each equation, m_b for the exponent interpolation and C_b for the coefficient interpolation. Therefore, is required leastwise one mixed mode testing data.

4.1 Fatigue Damage Evolution Model Proposed by Turon et al.

Turon et al. [3] published a breakthrough work, proposing a fatigue damage evolution model using the experimental results fitted by the Paris' law. In this way, linking the experimental data with the simulation scenario using the SERR. This procedure avoids the trial and error task necessary to fit the damage growth predicted by the FEM model against experimental results, as was done in the previously displacement based models. Furthermore, since the Paris' law parameters are fitted from the experimental data, it does not have the structure dependence of the others models. Eq. (17) shows the proposed fatigue damage evolution model.

$$\frac{dD^f_K}{dn} = \frac{dD^f_K}{dA^d_i} \frac{dA^d_i}{dn} \tag{17}$$

The derivative of the stiffness damage variable with respect to the damaged element area is obtained by Eq. (18) and the damaged area growth rate $\frac{dA^d_i}{dn}$ of the element is obtained by Eq. (19).

$$\frac{dD^f_K}{dA^d_i} = \frac{1}{A_i} \frac{\left[\delta^f_{eq}(1 - D_K) + D_K \delta^0_{eq}\right]^2}{\delta^0_{eq} \delta^f_{eq}} \tag{18}$$

$$\frac{dA^d_i}{dn} = \frac{A_i}{A_{cz}} \frac{dA^d}{dn} \tag{19}$$

The crack area growth rate $\frac{dA^d}{dn}$ is obtained by the Paris' law given by Eq. (12). For the estimation of the cohesive zone area, the model uses a cohesive zone length based on the closed-form solution developed by Rice [4] shown in Eq. (20). This equation was formulated for a pure mode I loading. However, the model also uses it for the mode II and mixed-mode loading.

$$l_{cz} = \frac{9\pi}{32}\frac{E_I G_I}{{S_I}^2} \tag{20}$$

Assuming a straight crack front, the cohesive zone area is found by multiplying the cohesive zone length l_{cz} and the RVE width b, as follows.

$$A_{cz} = b l_{cz} \tag{21}$$

Finally, substituting Eqs. (18), (19) and (21) into Eq. (17), the fatigue damage evolution model becomes:

$$\frac{\mathrm{d}D_K^f}{\mathrm{d}n} = \frac{1}{A_{cz}} \frac{\left[\delta_{eq}^f (1-D_K) + D_K \delta_{eq}^0\right]^2}{\delta_{eq}^0 \delta_{eq}^f} \frac{\mathrm{d}A^d}{\mathrm{d}n} \tag{22}$$

4.2 Fatigue Damage Evolution Model Proposed by Harper and Hallett

Harper and Hallett [5] studied the behaviour of the elements on the cohesive zone and observed two distinct regions. The first region, which is further away from the crack tip, is dominated by a quasi-static phenomenon while the second one, nearest to the crack tip, is dominated by fatigue. Fig. 4 shows the effect of this two zones on the traction-separation curve.

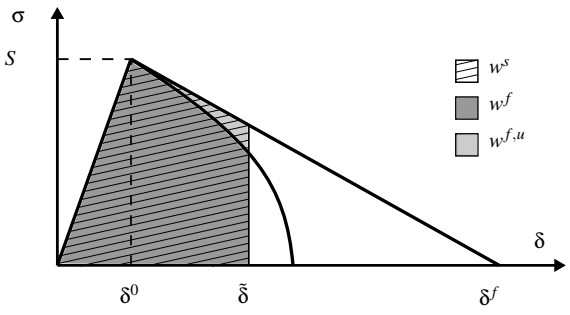

Fig. 4 Fatigue traction–separation response

In this model the fatigue damage rate is not directly proportional to the element crack length. Therefore, the fatigue damage rate is calculated by the chain rule as follows,

$$\frac{\mathrm{d}D_S^f}{\mathrm{d}n} = \frac{\mathrm{d}D_S^f}{\mathrm{d}l_{el}^d}\frac{\mathrm{d}l_{el}^d}{\mathrm{d}n} \tag{23}$$

where the first derivative term $\frac{\mathrm{d}D_S^f}{\mathrm{d}l_{el}^d}$ express the fatigue damage increment as a function of element crack increment and is given by Eq. (24)

$$\frac{\mathrm{d}D_S^f}{\mathrm{d}l_{el}^d} = \frac{1 - D_S^s - D_S^{f,u}}{l_{el}} \tag{24}$$

where the unwanted fatigue damage parameter $D_S^{f,u}$ is given as follows.

$$D_S^{f,u} = \frac{w^s - w^f}{0.5\,(\delta - \delta^0)\,S} \tag{25}$$

The second derivative in Eq. (23), $\frac{\mathrm{d}l_{el}^d}{\mathrm{d}n}$ correspond to element the crack growth rate is given by Eq. (26).

$$\frac{\mathrm{d}l_{el}^d}{\mathrm{d}n} = \frac{l_{el}}{0.5\left(\frac{G_{eq}}{G_{eq,c}}\right) l_{cz,c}} \frac{\mathrm{d}a}{\mathrm{d}n} \tag{26}$$

where $l_{cz,c}$ is the length of the cohesive zone for the critical point in quasi-static delamination growth, where the crack becomes unstable evaluated by a previous quasi-static analysis.

Finally, replacing Eqs. (24) and (26) into Eq. (23), results in a damage rate as follows.

$$\frac{\mathrm{d}D_S^f}{\mathrm{d}n} = \frac{1 - D_S^s - D_S^{f,u}}{0.5\left(\frac{G_{eq}}{G_{eq,c}}\right) l_{cz,c}} \frac{\mathrm{d}a}{\mathrm{d}n} \tag{27}$$

This strength-based damage parameter is converted to the stiffness-based damage using Eqs. (28) and (29).

$$D_K = 1 - \frac{\delta_{eq}^0}{\tilde{\delta}_{eq}}\,(1 - D_S) \tag{28}$$

$$\tilde{\delta} = \delta_{eq}^0 + D_S^s(\delta_{eq}^f - \delta_{eq}^0) \tag{29}$$

4.3 Fatigue Damage Evolution Law Proposed by Kawashita and Hallett

Kawashita and Hallett [6] improved the Harper and Hallett [5] model, on which three non-local aspects were added:

- Identification and tracking of the delamination front.

- Estimation of the element length in the direction of the crack propagation.
- The use of SERR at the failure point to calculate the crack increment.

The tracking algorithm works in two different stages. At the fatigue nucleation stage, it tracks the SERR peaks as the crack initiation elements. The fatigue propagation stage is characterised by the presence of at least one entirely failed element. In this case, the algorithm tracks the elements adjacent to the failed one to identify the elements located at the crack tip. The use of this approach allows the model to degrade only these elements instead of distributing the crack growth all over the cohesive zone, as is performed on the previous models.

Since this model degrades only the crack tip elements, there is no need to estimate both the cohesive zone length or the unwanted fatigue damage. Therefore, accounting only for the element effective length $l_{el,\phi}$ instead of the entire cohesive zone length and in the absence of any unwanted fatigue damage, Eq. (27) becomes:

$$\frac{\mathrm{d}D_S^f}{\mathrm{d}n} = \frac{1-D_S^s}{l_{el,\phi}}\frac{\mathrm{d}a}{\mathrm{d}n} \tag{30}$$

As the element damage increases, the SERR changes. For example, even for a constant load simulation, the degradation process results in an increase of strain within the elements, inherent to the stable increment process. This effect yields on a variation of the elemental SERR, and the element achieves the right SERR value only at final failure when the traction-separation curve is complete. To overcome that issue, the proposed model takes the maximum value of the element neighbours, including itself. Since that, when the crack is propagating, the crack tip elements will always have a fully damaged neighbour that can provide a stable and more accurate SERR.

5 Comparative Study

The material properties used in this comparative study is obtained from the experimental data published by Asp et al. [12]. In their work, three mode ratios were tested: the double-cantilever beam (DCB) test was used to obtain the mode I properties, the four-point end-notched flexure (4ENF) for mode II properties and the mixed mode bending (MMB) at $\phi_{II} = 0.5$. The specimens used in the tests were the HTA/6376C carbon/epoxy prepreg produced by HEXCEL using a lay-up of $[0_{12}//(\pm 5/0_4)_s]$, where the sign "//" refers to the plane of the artificial delamination. The dimensions were 150mm long, 20mm wide with two 12 layers arms, which represents 1.56mm thickness, and an initial crack length of 35mm. The laminate properties are given in Table 1. All material properties listed in Table 1 are from [12] except the fitting parameters (λ, η, C_b and m_b), the interfacial strength (S_I and S_{II}) and stiffness (K_I and K_{II}). The interfacial strength for mode II is calculated using the formulation proposed by Turon et al. [13], given by Eq. (31).

Table 1 Mechanical properties (HTA/6376C)

Layer Properties			
E_{11} (MPa)	120,000	$G_{23}(MPa)$	3,480
E_{22} (MPa)	10,500	$\nu_{12} = \nu_{13}$	0.3
G_{12} (MPa)	5,250	ν_{23}	0.51
G_{13} (MPa)	5,250		
Interface Properties			
$G_{I,c}$ (kJ/m^2)	0.26	C_I $(mm/cycle)$	2.21×10^{-3}
$G_{II,c}$ (kJ/m^2)	1.002	C_{II} $(mm/cycle)$	1.22×10^{-1}
$G_{0.5,c}$ (kJ/m^2)	0.447	$C_{50\%}$ $(mm/cycle)$	1.68×10^{-1}
λ	1.198	C_b	6.09×10^{5}
S_I (MPa)	30	m_I	5.09
S_{II} (MPa)	58.9	m_{II}	4.38
K_I (N/mm^3)	1×10^5	$m_{50\%}$	6.28
K_{II} (N/mm^3)	1×10^5	m_b	5.48

$$S_{II} = S_I\sqrt{\frac{G_{II,c}}{G_{I,c}}} \tag{31}$$

5.1 Finite Element Modeling

In the present work, for comparative purpose, the models are implemented into Abaqus explicit finite element software using 8-node hexahedron elements with one integration point. The local part of the algorithm is implemented in a user-defined material subroutine (VUMAT), and the non-local one is implemented in a VEXTERNALDB subroutine.

The laminate is represented by a 4-node shell plane strain element S4R while the cohesive zone

is modelled with a reduced integration solid hexahedron element C3D8R on which the constitutive model subroutine is applied. The element size on the direction of crack propagation is $0.1mm$, as shown in Fig. 5. A rigid tie contact is used to connect the upper and bottom laminate to the cohesive element. In the particular case of the 4ENF test, a single plane rigid element is modelled using R3D4 in order to transfer the load from the actuator to the specimen. A constraint is applied in the element edges at the translational through-thickness direction connecting the upper laminate to the rigid surface. The loads are applied according to the loading configuration proposed in Robinson et al. [1]. Fig. 6 shows the loading configurations.

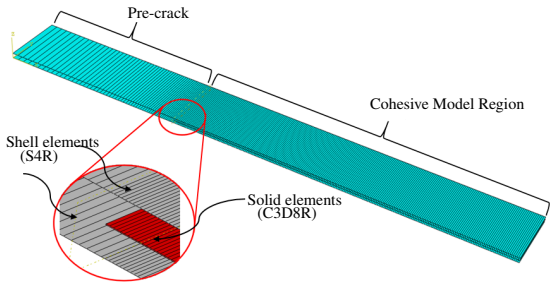

Fig. 5 Coupon mesh detail

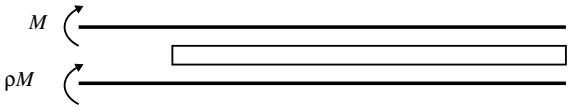

Fig. 6 Loading configurations

where,

$$G = 2\frac{3}{4\left(1+\frac{\sqrt{3}}{2}\right)^2}\frac{M^2}{bE_{11}I} \tag{32}$$

$$\rho = \frac{1-\frac{\sqrt{3}}{2}}{1+\frac{\sqrt{3}}{2}} \tag{33}$$

5.2 Results

Fig. 7 show the crack growth rate vs SERR variation to fracture toughness ratio for mixed mode at $\phi_s = 0.5$.

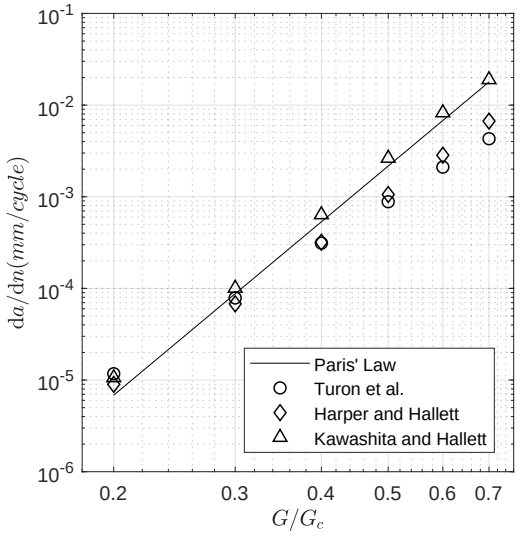

Fig. 7 Comparison between numerical prediction for the crack growth rate an experimental results for mixed mode fatigue induced delamination

In Fig. 7, Turon et al. [3] model shows a good result without the need for any fitting adjustment. For the Harper and Hallett [5] mode, the better estimation of the cohesive zone length combined with the strength-based model provides small improvement on the crack growth rate estimation. However, at high G/G_c value, both models present an unconservative error when compared to the Paris' law curve fitted from experimental data. The degradation of only the element in the crack tip performed in Kawashita and Hallett [6] model better represents the Paris' law idealisation of an effective main crack and promotes great improvements in the results shown in Fig. 7

5.3 Conclusion

The present comparative study found that the use of SERR-based Paris' law variation combined with CZM as proposed by Turon et al. [3] can simulate the high-cycle fatigue-driven delamination allowing the use of a slow growth approach in the damage analysis. Additionally, the strength-based model as performed by Harper and Hallett [5] promotes error reduction when compared with the stiffness-based one. Finally, The use of a crack tip tracking algorithm as pro-

posed by Kawashita and Hallett [6] promotes a more accurate result.

6 Acknowledgments

The authors acknowledge the financial support received for this work from the national research council CNPq, Grant 301053/2016-2 and 145467/2015-5, FINEP/CAPTAER II, Grant 0109020700 and FAPESP Grant 2015/16733-2.

References

[1] Paul Robinson, Ugo Galvanetto, Davide Tumino, Giordano Bellucci, and David Violeau. Numerical simulation of fatigue-driven delamination using interface elements. *International Journal for Numerical Methods in Engineering*, 63(13):1824–1848, 2005.

[2] R. H. J. Peerlings, WAM Brekelmans, R. De Borst, and M. G. D. Geers. Gradient-enhanced damage modelling of high-cycle fatigue. *International Journal for Numerical Methods in Engineering*, 49(12):1547–1569, 2000.

[3] A. Turon, J. Costa, P. P. Camanho, and C. G. Dávila. Simulation of delamination in composites under high-cycle fatigue. *Composites Part A: Applied Science and Manufacturing*, 38(11):2270 – 2282, 2007. CompTest 2006.

[4] J. R. Rice. The mechanics of earthquake rupture. In A. M. Dzieworski and E. Boschi, editors, *Physics of the earth's interior*, pages 555–649. Italian Physical Society and North-Holland Publ Co., 1980.

[5] Paul W. Harper and Stephen R. Hallett. A fatigue degradation law for cohesive interface elements - development and application to composite materials. *International Journal of Fatigue*, 32(11):1774 – 1787, 2010.

[6] Luiz F. Kawashita and Stephen R. Hallett. A crack tip tracking algorithm for cohesive interface element analysis of fatigue delamination propagation in composite materials. *International Journal of Solids and Structures*, 49(21):2898 – 2913, 2012.

[7] O. J. Nixon-Pearson, S. R. Hallett, P. W. Harper, and L. F. Kawashita. Damage development in open-hole composite specimens in fatigue. part 2: Numerical modelling. *Composite Structures*, 106:890–898, 2013.

[8] Maurício V. Donadon and Diogo P. Lauda. A damage model for the prediction of static and fatigue-driven delamination in composite laminates. *Journal of Composite Materials*, 49(16):1995–2007, 2015.

[9] Lin Ye. Role of matrix resin in delamination onset and growth in composite laminates. *Composites science and technology*, 33(4):257–277, 1988.

[10] J. D. Whitcomb and Langley Research Center. *Analysis of Instability-related Growth of a Through-width Delamination*. NASA technical memorandum. National Aeronautics and Space Administration, Langley Research Center, 1984.

[11] N. Blanco, E. K. Gamstedt, L. E. Asp, and J. Costa. Mixed-mode delamination growth in carbon-fibre composite laminates under cyclic loading. *International Journal of Solids and Structures*, 41(15):4219–4235, 2004.

[12] Leif E. Asp, Anders Sjögren, and Emile S. Greenhalgh. Delamination growth and thresholds in a carbon/epoxy composite under fatigue loading. *Journal of Composites, Technology and Research*, 23(2):55–68, 2001.

[13] A. Turon, P. P. Camanho, J. Costa, and J. Renart. Accurate simulation of delamination growth under mixed-mode loading using cohesive elements: Definition of interlaminar strengths and elastic stiffness. *Composite Structures*, 92(8):1857 – 1864, 2010.

7 Contact Author Email Address

Corresponding author: Lucas Amaro de Oliveira
E-mail: amaro@ita.br

Copyright Statement